Study on the Behavior of Atomic Layer Deposition Coatings on Nickel Substrate at High Temperature[1]

*Damoon Sohrabi Baba Heidary and Clive A. Randall

Center for Dielectrics and Piezoelectrics, Materials Research Institute, The Pennsylvania State University, University Park, PA 16802, USA

*Corresponding Author: Damoon Sohrabi Baba Heidary

Abstract

Although many techniques have been applied to protect nickel alloys from oxidation at intermediate and high temperatures, the potential of atomic layer deposition coatings has not been fully explored. In this paper, the application of ALD coatings (HfO_2, Al_2O_3, SnO_2, and ZnO) on Ni foils has been evaluated by electrical characterization and transmission electron microscopy analyses in order to assess their merit to increase Ni oxidation resistance; particular consideration was given to preserving Ni electrical conductivity at high temperatures. The results suggested that as long as the temperature was below 850 ^oC, the ALD coatings provided a physical barrier between outside oxygen and Ni metal and hindered the oxygen diffusion. It was illustrated that the barrier power of ALD coatings depends on their robustness, thicknesses, and heating rate. Among the tested ALD coatings, Al_2O_3 showed the maximum protection below 900^oC. However, above that temperature, the ALD coatings dissolved in Ni substrate. As a result, they could not offer any physical barrier. The dissolution of ALD coatings doped the NiO film, formed on the top of the Ni foils. As found by the electron energy loss spectroscopy (EELS), this doping affected the electronic transport process, through manipulating Ni^{3+}/Ni^{2+} ratio in the NiO films and the chance of polaron hopping. It was demonstrated that by using the ZnO coating, one would be able to decrease the electrical resistance of Ni foils by two orders of magnitude after exposing to 1020°C for 4

[1] This work has been published in Nanotechnology (link).

minutes. In contrast, the Al_2O_3 coating increased the resistance of the uncoated foil by one order of magnitude, mainly due to the decrease in ratio of Ni^{3+}/Ni^{2+}.

Keywords: ALD, diffusion, oxidation, conductivity, EELS, TEM, nickel

1. Introduction

The oxidation of nickel metal and its alloys has been studied for a long time [1,2]. Many coating techniques have been suggested to protect metals from oxidation, such as electrochemical plating[3], cladding and hardfacing [4,5], and organic films [6]. Recently, new coating techniques have been tried to preserve Ni from oxidation [7–9]. For example, graphene [10] and 2D BN [11] were coated on Ni foils, and it is shown that despite their thin thickness, they can effectively protect Ni metals from oxidation at high temperature in air. However, there is a temperature limit for effective protection against oxidation; graphene and 2D BN are both degraded at 650 [12] and 850 [13] ^{o}C, respectively.

Atomic layer deposition (ALD) is another new technique that has been widely used as a diffusion barrier on the various materials [11,14–19]. ALD coatings have been demonstrated as an effective gas barrier, due to the fact that they provide a continuous and conformal layer all around the object. The ALD encapsulating feature comes from the nature of their layer-by-layer growth process [20,21]. In spite of their potential to protect Ni metal from oxidation, the behavior of ALD coatings on Ni metals at high temperatures has not been thoroughly studied. Since many chemical compounds can be deposited by the ALD process [21], there are a number of potential candidates to preserve Ni from oxidation at high temperature.

The effective coating in order to protect nickel from oxidation has many applications[22], from turbine blades[23] to Ni foil passivation for growing piezoelectric films [24] and multilayer applications, such as Ni electrodes being used in co-fired capacitive devices, and multilayer piezoelectrics with lead free chemistries [25–27] and solid oxide fuel cells [28,29]. As a model system, nickel and $BaTiO_3$ cofiring

has been studied many times and underpins a multibillion dollar passive component industry[30–34]. A technique that can keep the Ni electrode metallic (i.e. preserve the conductivity of the Ni electrode) during the cofiring process in air or relatively oxidized atmospheres is very attractive for increasing performance and reducing manufacturing costs[35].

In this research, two measures were considered to kinetically limit the oxidation of the Ni metal. The key solution is the application of ALD coatings around Ni metal to make a physical barrier between Ni metal substrate and atmospheric oxygen. The second one is the fast heat treatment of Ni metals with fast heating and cooling rates. Thus, the Ni metal is exposed to high temperature a shorter amount of time. The fast heat treatments can be useful in sintering of Ni particles, in which Ni particles need to be exposed to high temperature for a short duration.

An ALD coating suitable for the present purpose, besides having small diffusion coefficient of oxygen, should have a good mechanical stability (i.e., no cracking due to strain) to remain continuous and flawless at high temperature, e.g. 1000 ^{o}C. As observed in our previous work [36], the barrier power of the ALD coatings against hydrogen gas [37,38] and humidity[39] decreases due to cracks and crystalline defaults. The source of strain for cracking can be the difference of thermal expansion between substrate and coating[40–42].

In order to make a complete introduction, it should be pointed out that the ALD coatings can be dissolved in the Ni foil substrate above some critical temperature. This phenomenon will be demonstrated later in this paper. So, the dissolution of ALD coating should be considered as the second mechanism, by which ALD coating collapses and cannot provide a physical barrier between the Ni foil and outside atmosphere.

These factors make the selection of ALD coatings a critical part of this study. Conventionally, HfO_2[43] and Al_2O_3[14] coatings are well-known gas barriers with amorphous structure. In addition,

SnO_2[44] and ZnO[36] coatings can be a potential candidate, since they can have a crystalline structure, and their cations provide 2+ oxidation state (Sn has the possibility of both 2+ and 4+ oxidations[45]).

In this study, we intended to investigate the behavior of ALD coating on Ni metals at high temperature and specifically determine how the electrical resistance of the coated Ni foils would be affected during a heat treatment.

2. Experimental procedures

Ni foils with purity of 99.5%, obtained from Alfa Aesar, were cut to 7×10 mm pieces, and two holes with diameter of 0.5 mm were drilled into some of them, as shown in Figure S1. The foils were cleaned in a supersonic bath of acetone for 5 minutes, followed by another 5 minutes in isopropyl alcohol, and dried in an oven for 20 minutes at 120 ^{o}C. Then, they were coated with the Al_2O_3, HfO_2, ZnO, and SnO_2 in the ALD system (Cambridge System, Savannah 200). The process recipes are shown in *Table 1*.

Table 1 ALD recipes for ZnO, Al_2O_3, SnO_2, and HfO_2 coatings

	ZnO	Al_2O_3	SnO_2	HfO_2
Metal-Precursors	DEZ*	TMA**	TDMA-Sn†	TDMAH††
Precursor dose time (s)	0.015	0.03	0.05	0.15
Purge time (s)	10	10	10	10
Water dose time (s)	0.015	0.1	0.1	0.03
Purge time (s)	10	10	10	10
Temperature	200 ^{o}C	200 ^{o}C	200 ^{o}C	200 ^{o}C
Growth rate	1.3 $\dot{A}/cycle$	0.9 $\dot{A}/cycle$	1.1 $\dot{A}/cycle$	1.1 $\dot{A}/cycle$
Base pressure	300 mtorr	750 mtorr	400 mtorr	400 mtorr

*Diethylzinc **Trimethylaluminum †Tetrakis(dimethylamino)tin(IV) †† Tetrakis (dimethylamido) hafnium (IV)

To study the oxidation behavior of the foils during the heat treatments, two platinum wires were passed through those holes, shown in Figure S1, and the samples were suspended in a tube furnace, by which temperature was increased at the rate of 4 ^{o}C/min to 900^{o}C in air, and DC resistance was measured during heating. Since the resistance due to formation of the Ni oxide film is much higher than the contact resistance and the other resistivities, the formation of NiO oxide layer can be traced online by monitoring the resistance of the foils.

A fast-heating furnace[46], which was able to heat up and cool down at the rate of 100 and -50 ^{o}C/min, was used to study the effect of the heat rate on the oxidation of the foils. The fast heat treatments were designed to investigate the effect of sintering condition on the ALD coating on Ni substrate. So, obviously, there was a need to assess the conductivity of Ni foils after a real sintering process. Based on the other studies on sintering Ni particles [47–50], the heating schedule of 1020^{0}C for 4 minutes was selected, and then it was confirmed that Ni particles could be successfully sintered with it. This heat treatment would be used as a criterion to evaluate the merit of the ALD coatings to preserve Ni conductivity during sintering of Ni particles.

Impedance spectroscopy tests were executed by Solartron Module Lab XM on the foils after the fast sintering to estimate the thickness of the oxide layers or the effectiveness of ALD coatings. The test was executed at the voltage of 1V and the range of 0.1 Hz to 10^5 Hz. To make sure that there is a good contact between the probe and the foils, a circular area with diameter of 3 mm on both sides of foils was sputtered by gold with thickness of 50 nm. After that, the foil was placed in a fixture and the impedance spectroscopy test was executed at room temperature.

The Transmission Electron Microscopy (TEM) samples and cross sections were prepared by FEI Helios NanoLab 660. TEM analyses were done by FEI TALOS F200X and JEOL-2010 field emission TEM,

equipped to Energy Dispersive X-ray Spectrometer (EDS) and electron energy loss spectroscopy (EELS) systems.

3. Results and Discussion

3.1 Nickel oxidation

The resistance of the uncoated Ni foil as a function of temperature during heating, at the rate of 4^{o}C/min in air, is shown in Figure 1 (a). The resistance is small at temperatures below 710^{o}C, but it starts to increase abruptly around 710^{o}C. As shown in Figure S2 in Supporting Information, the diffusivity of oxygen in NiO start to increase abruptly around 700^{o}C, and that causes an abrupt growth of NiO film, which is manifested as a rapid increase in the resistance. Nowotny and Sadowski[51] used a similar method to measure the diffusion coefficient of oxygen in NiO. Thus, the DC resistance measurement during heating can offer a strong tool to monitor the thickness of NiO film.

From now on, the temperature in which the resistance of Ni foil passes 10 Ω is called the critical temperature (T_0). By obtaining T_0 for the coated foils, one can judge the effectiveness of the ALD coatings on hindering oxygen diffusion. In other words, T_0 shows how protective a coating is against oxygen diffusion for ALD coating with similar chemistry (at the end of this paper, it will be shown that the ALD coatings can be dissolved in the NiO foil and affect the conductivity mechanism; thus, this test is only valid for comparison of the ALD coatings with a similar chemistry).

To further study the nature of T_0, a Ni foil was heated up to 700^{o}C, and just before increasing resistance, it was cooled down. The maximum measured resistance was 4 Ω. The TEM analysis was performed on this foil and compared with an untreated foil. *Figure 1* (b) shows the TEM micrograph of the untreated foil. As seen, an oxide layer can neither be observed nor detected with the EDS in the scale shown in this micrograph. On the other hand, there is an oxide layer with minimum thickness of 500 nm on the foil, heated to 700 ^{o}C, as presented in *Figure 1* (c) and (d). One can argue that this thickness (i.e.

~500 nm) is the minimum sensitivity limit of our in-situ measurement since the rise in resistance is high enough at this thickness so that our setup would be able to detect it. In addition, for clarity, it should be noted that the resistance difference between the coated foils and the uncoated foil before the heat treatments was too low, so that their difference is in the margin of error of this technique. As suggested here, and will be supported later, the NiO film should be thicker than ~500 nm for us to measure a resistance above 10 Ω for both coated and uncoated foils.

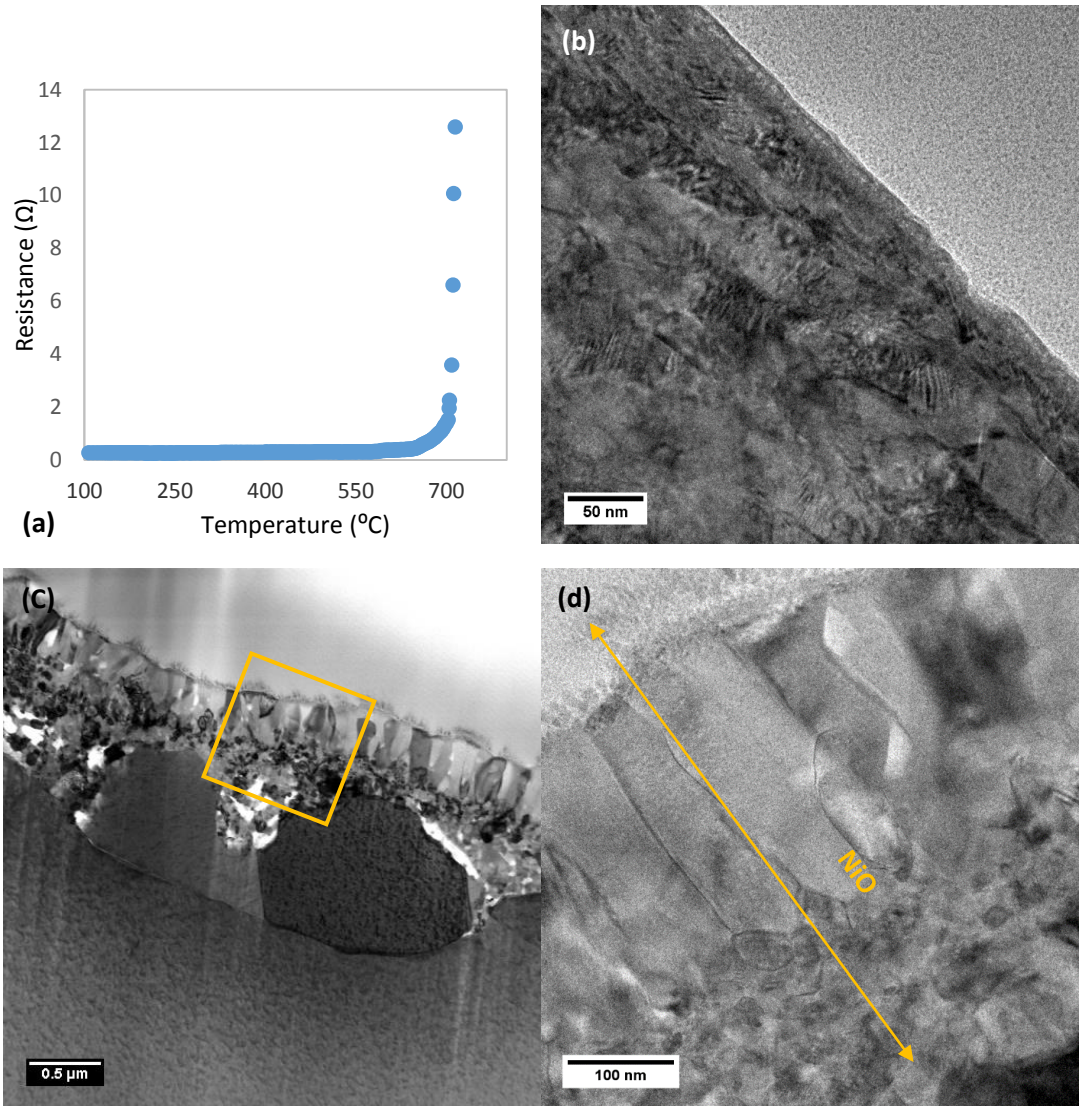

Figure 1. (a) resistance of nickel foil vs temperature. TEM micrograph from (b) nickel foil without any heat treatment, (c), (d) nickel foil, heated up to 700 °C with heating rate of 4 °C/min at different magnifications.

The second conclusion of the above TEM analysis is that Ni foils can tolerate some oxidation without a significant increase in resistance. The resistance below 10 Ω can be considered low in the context of the present study. So, eventually, this study narrows down to finding methods to hinder the growth kinetic of the NiO film to keep the resistance of Ni foils low. However, later, it will be shown that the doping of the NiO film with the suitable cations can be the other mechanism to lower the resistance.

In the rest of this paper, the fast heating rate and ALD coatings are explored to see their relative effectiveness in hindering the elevation of resistance during heat treatments.

3.2 ALD coatings and fast heat treatments

Figure 2 (a) presents the effect of HfO_2 ALD coating on the elevation of resistance at the heating rate of 4^{o}C/min. T_0 has been increased from 710 ^{o}C to 820 ^{o}C from the uncoated foil to the one coated with 35 nm of HfO_2, and then it decreased to 755 ^{o}C in the thickness of 50 nm. Based on the previous discussion, the higher critical temperature (T_0) means a coating with higher potential to preserve Ni conductivity. So the barrier power of HfO_2 coatings increases up to 35 nm and then decreases. *Figure 2* (b) shows the critical temperatures for HfO_2, Al_2O_3, ZnO, and SnO_2 coatings with different thicknesses. As is illustrated in this plot, the same trend has been noted in all the ALD coatings. The increase of critical temperature (T_0) by thickness is due to the fact that the thicker layer can provide a more effective barrier against oxygen diffusion, as previously reported [36]. On the other hand, the thicker ALD coatings are more susceptible to cracking, which provides an easy path for diffusion, as demonstrated by Jen et al [41,40]. So there is a critical thickness in which both diffusion barrier and mechanical stability (i.e., no cracking due to thermal strains) are high enough to provide the maximum protection. The highest T_0 (i.e., the most effective barrier) was found to be 850 ^{o}C for the foil, coated with 35nm of SnO_2. The second highest T_0, 835 ^{o}C, belongs to ZnO with thickness of 25 nm.

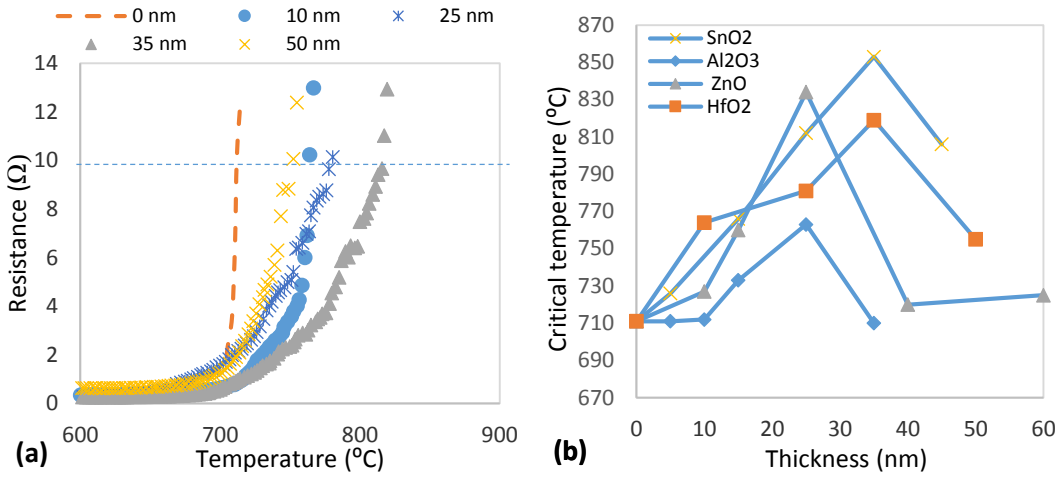

Figure 2 (a) Resistance vs. temperature for Ni foils coated with different thickness of HfO_2 and heated with the rate of 4°C/min. (b) Critical temperature vs. thickness for the foils with the different ALD coatings.

The second approach to hindering the formation of NiO film is fast heat treatments. By heating and cooling quickly, the exposure time to high temperature is shorter, and the NiO film is thinner. For example, the resistance of a nickel foil, heated up to 800 ^{0}C with rate of 100 ^{0}C/min and then immediately cooled down with the rate of -50 ^{0}C/min, was 2Ω. Thus, T_0 can be increased from 710 ^{0}C at the heating rate of 4 ^{0}C/min to above 800 ^{0}C by utilizing the fast heat treatments. As explained in the Introduction, the fast heat treatment can be used for sintering Ni particles, in which the Ni particles are exposed to high temperature for a short duration of time. The study of the behavior of the coated Ni foils during these heat treatments can provide insights on the behavior of the ALD coating on Ni particles.

For the foils subjected to the fast heat treatment, the *in situ* resistivity measurements were not technically available. So their resistance was measured by impedance spectroscopy after the heat treatments. Impedance spectroscopy can provide information about electron hopping and NiO film thickness.

Figure 3 (a) shows the impedance vs frequency for the foils, heated to 900, 1000, and 1100 ^{0}C at the rate of 100 ^{0}C/min. For all the foils, impedance (Z) increased by decreasing frequency and eventually reached a plateau at some critical frequencies. To explain this behavior, the Ni foil can be thought of as

two impedance elements of Ni metal and NiO film, which connected to each other in series. The impedance of Ni metal is negligible, so the total impedance is correlated to the impedance of NiO film. Since electron hopping between Ni^{3+} and Ni^{2+} is the dominant conductivity mechanism in the NiO film [52,53], the impedance is increased by decreasing frequency linearly in log scale and eventually, when the frequency is low enough, the hopping will not be an effective conductivity mechanism, and impedance becomes constant vs frequency. The constant impedance, shown as Z_0, can be reliable criteria for evaluating the thickness of NiO film and the effectiveness of hopping mechanism. Snowden and Saltsburg [54] observed the same linearity and plateau for impedance spectroscopy of nickel oxides.

The Z_0 was measured for the foils with different ALD coating, heated to 900, 1000, and 1100 ^oC, and the results were shown in *Figure 3* (b) along with the Z_0 of the uncoated foil. At 900 ^oC, the Z_0 was 6 Ω, 70 Ω, 370kΩ, and 901 kΩ for Al_2O_3, HfO_2, ZnO, and SnO_2, respectively. The difference of those points are not recognizable in the scale of the plot in *Figure 3* (b). The Z_0 of the uncoated foil was 13.5MΩ, so all the ALD coating could decrease the resistance considerably, and the Al_2O_3 coating seemed the best candidate for doing that. However, by raising the maximum temperature to 1000 and 1100 ^oC, the impedance of the Al_2O_3-coated foil significantly increased even more than the uncoated foil. The impedance of the HfO_2-coated foil considerably increased as well, but it did not pass the impedance of the uncoated foil. The least impedance growth was detected in ZnO and SnO_2-coated foils. This behavior would be explained by the result of TEM analyses.

In order to evaluate how effective ALD coatings are after a real sintering schedule, the coated Ni foils were exposed to the designed sintering schedule, explained in the Experimental section, and then the impedance spectroscopy was performed on them; the results are shown in *Figure 3* (c). The lowest resistivity or maximum protection was obtained for the ZnO-coated foil. All the ALD coatings show a level of protection; however, again the anomaly is the foil coated with Al_2O_3.

Figure 3 (d) shows the result of impedance spectroscopy on the SnO_2-coated foils with different thicknesses after the sintering heat treatment. The maximum protection has been found for the coating with 15 nm thickness. This outcome can be contrasted by the data in Figure 2 (b), which illustrate that the maximum protection at the slow heating rate is obtained for the SnO_2 coating with 35 nm thickness. As mentioned before, there is balance between mechanical stability (i.e. no cracking due to strain) and diffusion barrier of ALD coatings, which results in an optimum thickness. By increasing heating rate, the importance of the mechanical stability is promoted over the diffusion barrier, and the thinner coatings are more mechanically stable, according to Jen et al.[41,40]. So the optimum thickness will be smaller in fast heating rate than the optimum thickness in slow heating rate. This phenomenon has been observed in other studies. For example, Li et al. [13] demonstrated that the oxidation resistance of 2D BN coating depends on heat treatments.

As indicated by the data in *Figure 3*, the resistance (i.e., impedance at low frequency) values for the coated foils exposed to the sintering heat treatment are not low enough to serve as an electrode; one may expect that electrodes have a resistance below 10 Ω after sintering, while the measured resistances were on the order of MΩ. However, the two-orders-of-magnitude decrease in resistance, as shown in *Figure 3* (c), indicates a significant potential in the ALD coatings to reduce the Ni foil resistance. So it would not be trivial to investigate the evolution of the ALD coatings during ramping to high temperature by TEM analyses.

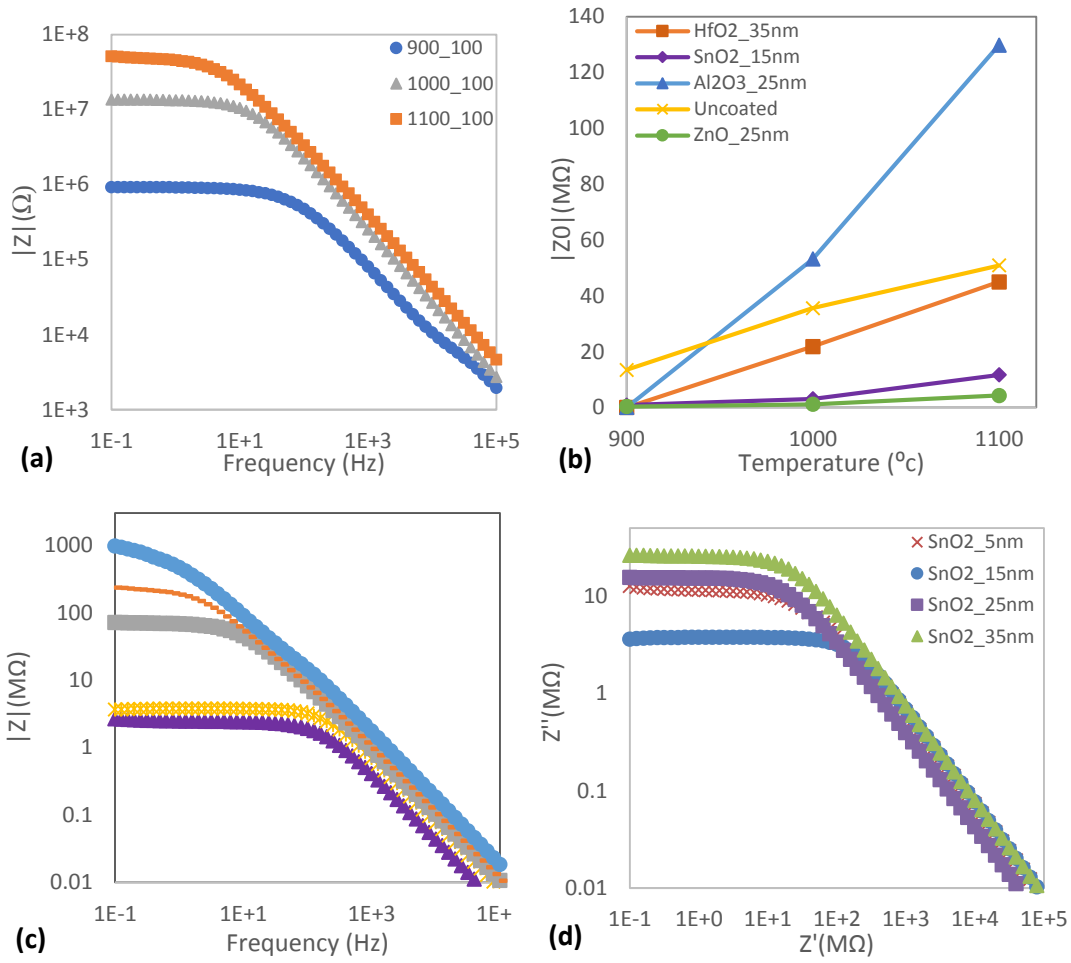

Figure 3 (a) Total impedance (Z) vs frequency for the uncoated foils, heated to 900, 1000, and 1100 °C; (b) Impedance at low frequency (Z_0) vs temperature for different ALD coatings. Z vs frequency for the coated foil with (c) different ALD coating and (d) SnO_2 coating with different thicknesses.

3.3. TEM Analyses

3.3.1 TEM Imaging

In order to investigate the behavior of the ALD coating during the heat treatments, the STEM (scanning transmission electron microscopy) micrographs of the Al_2O_3-coated foil heated to 700, 900, and 1100°C at the rate of 100 °C/min together with as-coated foil, are presented in *Figure 4*. It can be seen that the ALD coating remains on the top of the foil without any discontinuity or major defect until 700°C. However, at 900 °C, Ni atoms diffuse through the ALD coating, and the ALD layer is buried under the Ni

substrate, as shown in *Figure 4* (c). At 1100 °C, the ALD layer is dissolved in the foil. The different regions, detected by EDS analyses, are labeled in the micrographs.

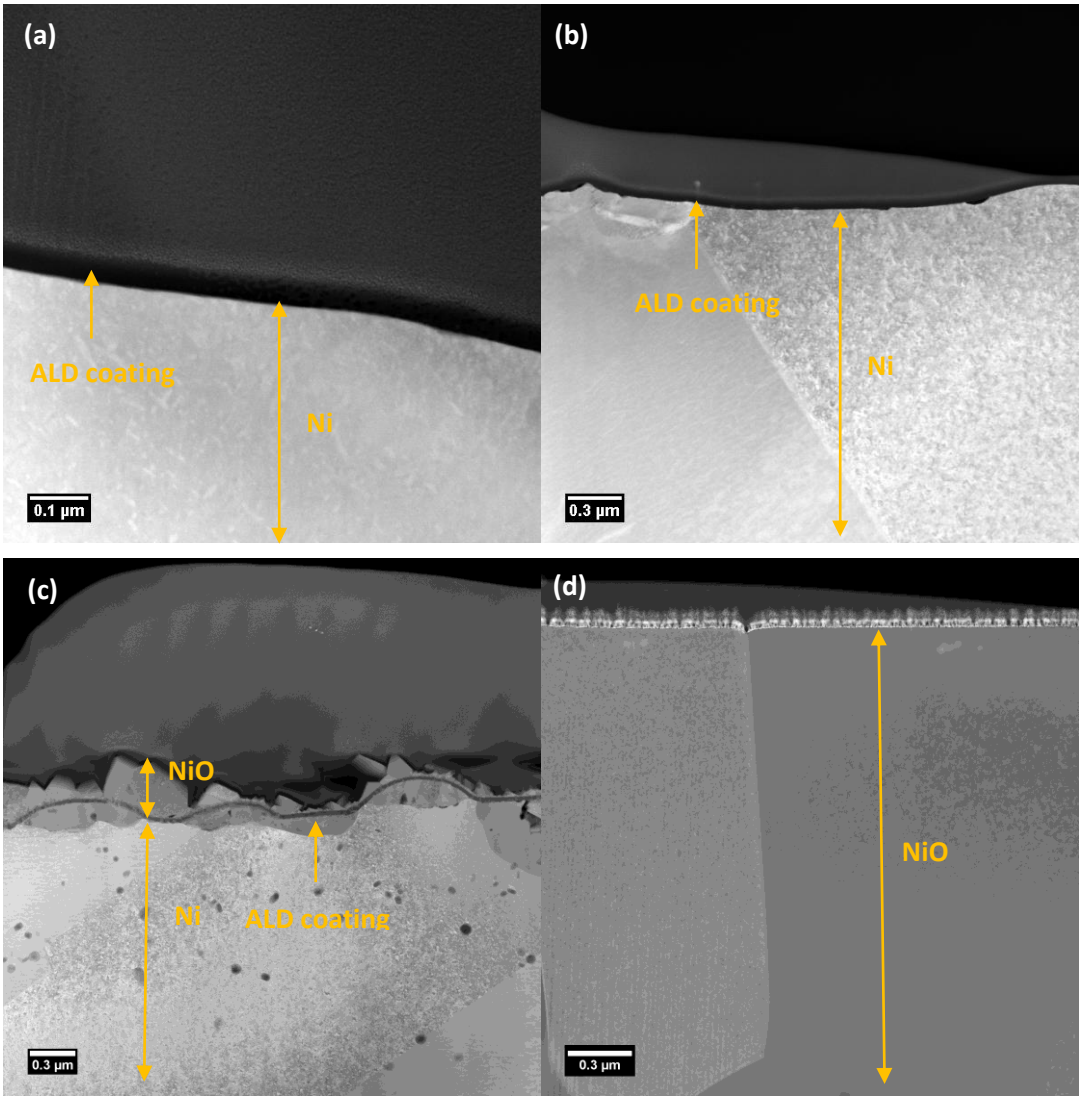

Figure 4 HAADF-STEM micrographs of the Al_2O_3-coated nickel foil in (a) as-coated condition, and after heating to (b) 700, (c) 900, and (d) 1100 °C and cooling down without holding with the rate of 100 and -50 C/min, respectively.

Since the Al_2O_3 coated foil seems to be at a transition point at 900 °C, it was studied more carefully, and more TEM micrographs are presented in *Figure 5*. The first observation is that the ALD layer is crystalized due to the presence of Moiré fringes[55] in *Figure 5* (a). In addition, the x-ray diffraction (XRD) pattern with grazing incidence diffraction geometry shows an extra wide peak at 68°, which was absent in the diffraction pattern with conventional Bragg-Brentano geometry. The extra peak is well matched

with one of the corundum peaks. The XRD pattern unambiguously showed Ni and NiO phases in the foil. The XRD pattern is shown in Figure S3 of Supporting Information.

In order to bury the ALD layer, Ni atoms need to pass though the ALD layer. Their diffusion path can be clearly illustrated by the bright field STEM micrographs, in which the Al_2O_3 coating appears bright and the Ni atoms dark. The dark narrow line passing through the ALD layer are the cracks or grain boundaries, which provide easy pass for Ni atoms. This explanation can be further supported by EDS maps of the ALD coating presented in *Figure 5* (c). The EDS Ni map shows some thin lines of Ni in the ALD layer, indicating that Ni concentration in these lines is above the detection limit of the EDS instrument. These lines are detected with different contrast in the counterpart of HAADF micrographs. In addition, some parts of the Al_2O_3 layer started to dissolve in surrounding NiO phase. *Figure 5* (d) shows some parts of the ALD coating, where the border between the ALD coating and NiO phase is fuzzy, in the right-hand side of the micrograph. In comparison to the border in left-hand side, one may conclude that the ALD coating is in the early stage of the dissolution process. *Figure 5* (e) is the dark field TEM micrograph. The micrograph was formed by selecting one of the bright spots in the diffraction pattern, shown in the inset. The fact that the grain on the top is bright and the other NiO grains are dark demonstrates that the bright grain has different crystal orientation from the rest of the grains. This grain is shown in the *Figure 5* (b) with an arrow. It may be concluded that the Ni diffuse through the coating and then re-nucleate on the top of it in the different crystal orientation. This is why ALD coating seems to be buried under the Ni substrate. In addition, as is indicated by EDS maps, oxygen can pass through the ALD coating and oxidized Ni underneath it.

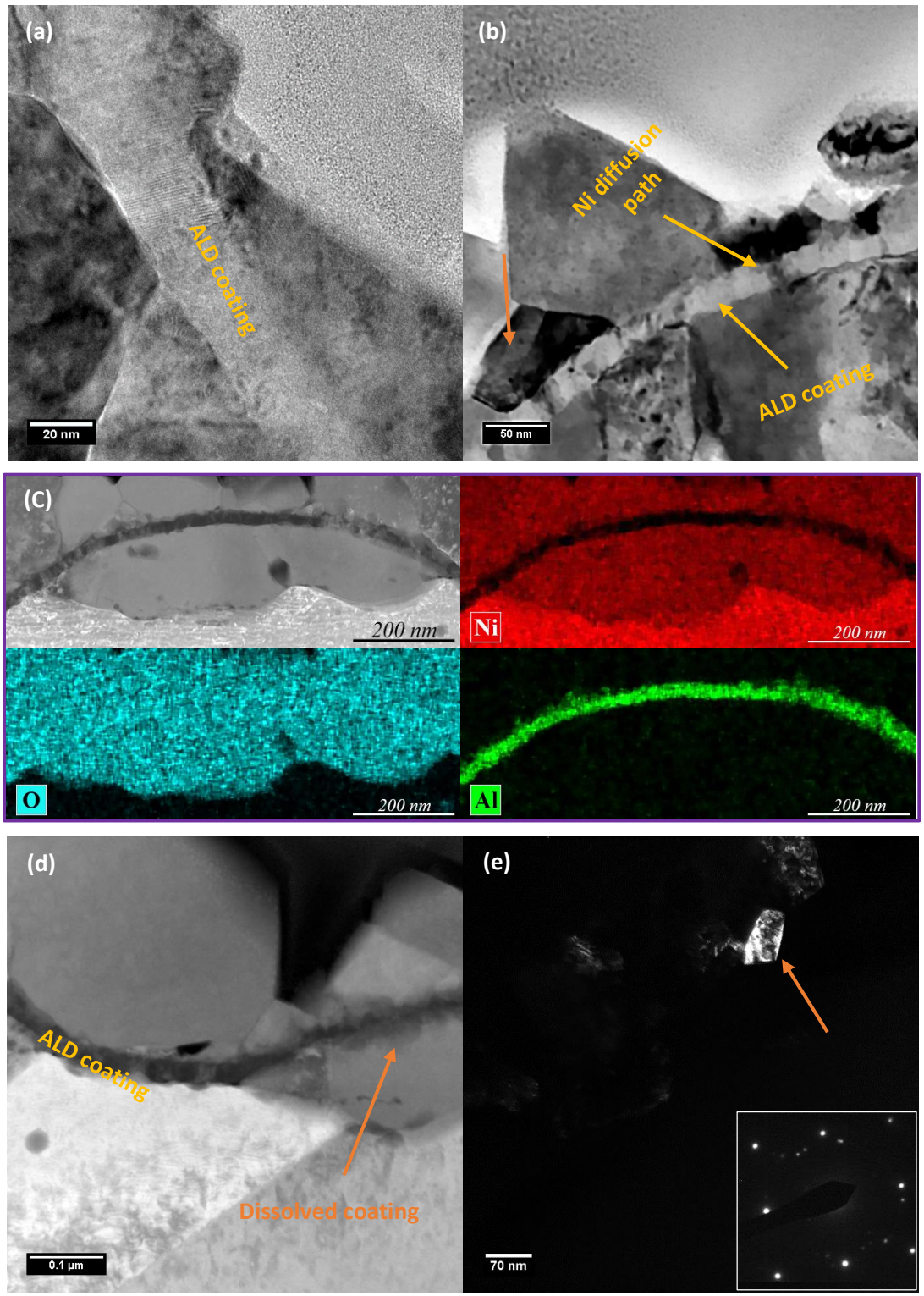

Figure 5 (a) TEM, (b) STEM Bright Field, (c) EDS maps and HAADF (d) HAADF, and (e) TEM dark field micrographs of the nickel foil coated with 25 nm of Al_2O_3 and heated to 900°C.

Figure 6 shows the STEM micrograph of the HfO_2 and SnO_2 coatings after exposure to the same heat treatment (heating to 900^oC at the rate of 100^oC/min and immediately cooling down at the rate of -50^oC/min). The HfO_2 coating is buried under the NiO substrate, as was the case for the Al_2O_3 coating. The EDS map of the HfO_2 layer is presented in Figure S4 in Supporting Information. *Figure 6* (c, d) show the SnO_2-coated foil after the same heat treatment. The SnO_2 coating disappeared, and the EDS analyses did not show any peak for Sn. However, one should bear in mind that the detection limit of STEM-EDS was reported 1-2 wt%[56] in average working conditions. The SEM micrographs of the ZnO-coated foil, presented in Figure S6, did not show any sign of the ALD coating after the same heat treatment either.

Two scenarios can be thought of for the disappearance of ZnO and SnO_2 ALD coating. Either the ALD coatings were evaporated during the heat treatment, or they were buried under the Ni film and dissolved into it before 900^oC. The former scenario does not seem the dominant mechanism, since it does not provide any explanation for the decrease of resistance in both SnO_2 and ZnO coated foils. In addition, Varela et al. [45] demonstrated that the SnO_2 evaporation is limited above 1200 ^oC, and Badev et al. [57] showed that the weight loss of ZnO nanopowder is less than 0.4 wt.%, even after one hour holding at 900 ^oC. So the second scenario is more likely, and both SnO_2 and ZnO dissolved into NiO film. This conclusion will be further supported by EELS data.

Since all the foils were exposed to the same heat treatment (i.e. heating to 900 ^oC by the fast heat treatment), the thicknesses of NiO film can be an indicator of how effective the ALD coating is to hindering the mass transfer of Ni and oxygen atoms. The thickness of NiO films was 0.26, 0.647, 1.16, and 1.32 µm for the foils coated with Al_2O_3, HfO_2, SnO_2, and ZnO. The FIB cross section of the uncoated foil, exposed to the same heat treatment, showed that the thickness of the NiO film was 1.95 µm, as illustrated in Figure S6 in Supporting Information. One can conclude that all the ALD coatings offer some level of diffusion barrier against oxygen; the Al_2O_3 coating has the highest barrier power and ZnO the lowest.

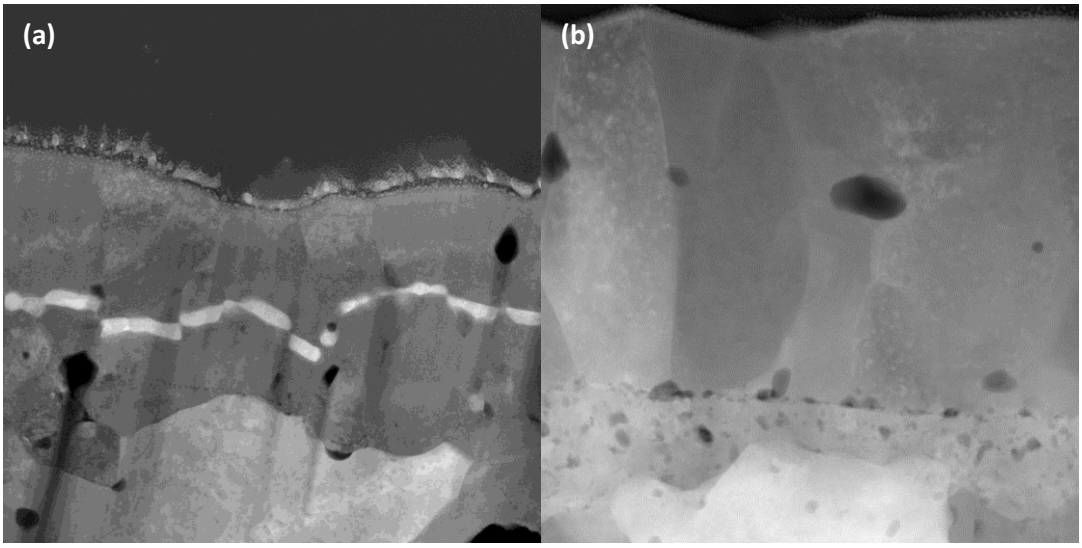

Figure 6 HAADF-STEM micrographs of the foils, coated with 25nm of (a) HfO_2 and (b) SnO_2 after heating to 900°C with the fast heat treatment.

3.3.2 EELS analyses

The foil, coated with Al_2O_3, showed an abnormal increase in the impedance after exposing to 1020 ^oC for 4 minutes. As shown in Figure 3(c), its impedance is even higher than the impedance of the uncoated foil. On the other hand, the Al_2O_3 coatings can hinder oxygen diffusion even more effectively than the other ALD coatings (e.g. the ZnO-coated foil), as suggested above. One may expect that the foil with less oxygen diffusion has a thinner NiO film and, consequently, should have lower impedance than that of the other foils. However, the reason for the large impedance of the Al_2O_3-coated foil can be explained by the study of NiO defect chemistry.

Nickel oxide has the possibility of non-stoichiometric defects with Ni vacancies (V_{Ni}'') [54,58,59], whose concentration depends upon the amount of oxygen exposure to the Ni metal during oxidation [60,61]. It was reported that the non-stoichiometric solubility can be $Ni_{1-\alpha}O$ with $0<\alpha<0.2$ [62]. The V_{Ni}'' species introduce negative charge to the system, and at the same time, the charge neutrality should maintain in the oxide. Thus, some of Ni ions change their oxidation state from 2+ to 3+ to electronically

compensate for the extra negative charge. The larger ratio of Ni^{3+}/Ni^{2+} increases the chance of electron hopping in NiO and decreases its resistance.

The EELS point analysis was done on the uncoated, 25nm-Al_2O_3-coated, and 25nm-ZnO-coated foils after heating to 1100 ^oC. The raw data are presented in *Figure 7* (a - c). The points were on the top, 1/3, 2/3, and the bottom of the NiO films. The ratio of the height of L_2 edge over L_3 edge after the background subtract is equal to the Ni^{3+} concentration over Ni^{2+} concentration [60,63,64]. This ratio was calculated as $\frac{L_2-base\ line}{L_3-base\ line}$ and is shown as L* in *Figure 7* (d). The results suggest that there is a high concentration of Ni^{3+} on the top of the film, and it decreases toward the interface of Ni and NiO in all three samples. This is due to the fact that the excess of oxygen causes more (V_{Ni}'') in NiO [61], and oxygen ions diffuse inside the foil from the top to the bottom, so that there is a gradient of oxygen concentration across the NiO films. As a result of this oxygen gradient, Ni^{3+} has the maximum concentration at the top of the foil and decreases toward the interface. This observation matches well with the Voleník et al. [61] work on nickel oxidation and Tyuliev and Sokolova [60] EELS analyses regarding Ni^{3+} concentration at NiO surfaces. Thus, EELS provides a powerful tool to trace the concentration of Ni^{3+}, which has a direct influence on conductivity due to electron hopping between Ni^{2+} and Ni^{3+}. It should be noted that EELS analyses are more suitable for detecting atoms with low concentration than EDS analyses, since they are able to provide a higher signal-to-noise ratio [65]. This is especially true for the atoms with low atomic mass[56].

Now, one can hypothesize that in the Al_2O_3 coating, Al^{3+} is dissolved into NiO film and then, to maintain charge neutrality, the system would decrease the concentration of Ni^{3+}. This decreases the chance of hopping between Ni^{3+} and Ni^{2+} and increases impedance, as shown in *Figure 3* (c). This hypothesis can be supported by the curve of Al_2O_3 in *Figure 7* (d). The fact that the NiO film of the Al_2O_3-coated foil has lower L* on the top than that of the uncoated foil suggests a lower concentration of Ni^{3+} in the presence

of Al^{3+}. In contrast, the ZnO curve is above both the uncoated and the Al_2O_3-coated foils, especially on the top of the NiO film. This is due to the fact that both Ni^{3+} and Ni^{2+} can be replaced by Zn^{2+}. If Ni^{2+} is replaced by Zn^{2+}, the number of the total 2+ charges is constant, and the charge neutrality is maintained. However, if Ni^{3+} is replaced by Zn^{2+}, more Ni^{3+} should be created due to the charge neutrality. This is the reason that the L* is higher in the ZnO-coated foil, and this can thereby contribute to their low resistivity. It is worth mentioning that L* of all three foils have almost the same values at the Ni-NiO interface, indicating Ni^{3+}/Ni^{2+} ratio is same when Ni and NiO is at equilibrium. In addition, Muto et al.[64]found the ratio of L_2/L_3 0.25 for stoichiometric NiO. Their finding matches well with the L* in *Figure 7* (d) at the interface. This can support the validity of our EELS analyses.

Due to the lattice charge neutrality, required during ionic diffusion, the charge balance of cations with 4+ state would limit their diffusivity in the NiO grains. So Hf^{4+} [66] and Sn^{4+} [45,67] have small diffusion coefficients in NiO crystal. One can argue that since the ions with 4+ states do not effectively diffuse into the NiO crystal structure, they cannot change the ratio of Ni^{2+}/Ni^{3+}; this is why the resistance of the HfO_2-coated foil does not significantly rise in comparison to Al^{3+} in the plot of *Figure 3* (b and C). However, Varela et al. [45] argue that the oxidation state of Sn changes from 4+ to 2+ in SnO_2 above 1000 ^oC. If this is the case, Sn^{2+} can decrease the resistance of NiO film in the same mechanism, which was explained for Zn^{2+}. This explanation can justify the one-order-of-magnitude decline in resistance by going from HfO_2 coatings to SnO_2 coatings in *Figure 3* (c) and why the graph of SnO_2 and ZnO coated foils sit next to each other.

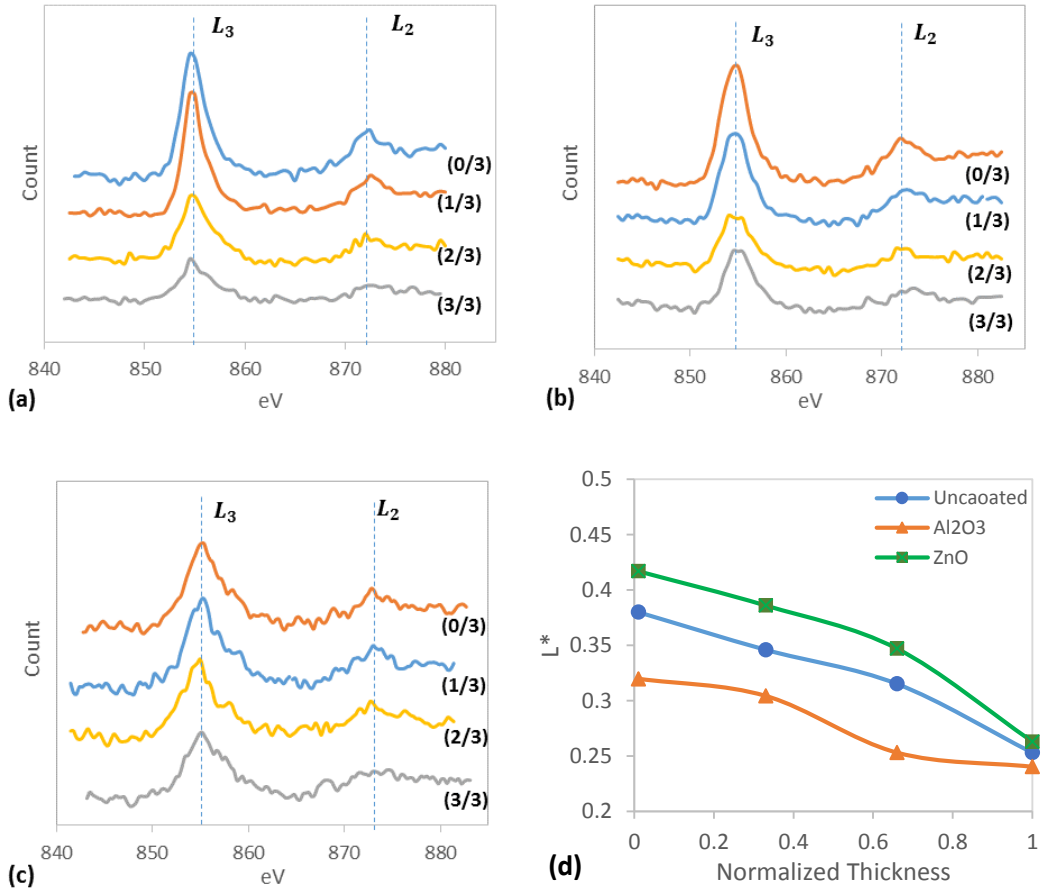

Figure 7 EELS spectra of nickel $L_{2,3}$ edges, taken from nickel foil (a) uncoated and coated with (b) Al_2O_3 and (c) ZnO ALD on top, 1/3, 2/3, and the bottom of NiO film after exposure to 1100°C. (d) L, which is $\frac{L_2-base\ line}{L_3-base\ line}$, versus normalized width of the NiO film.*

Now one can explain the impedance of the coated foil, reported in previous section in *Figure 3* (b). The Al_2O_3-coated foil has the lowest impedance at 900 °C since the Al_2O_3 coating can effectively prevent the oxygen diffusion. The thickness of NiO film was 0.26 µm and, consequently, the impedance was 6 Ω. However, at temperature above 900 °C, the Al_2O_3 coating would be dissolved in the NiO film and significantly increase the impedance. On the other hand, the ZnO coating cannot hinder oxygen diffusion as effectively as the Al_2O_3 at 900°C. This is why the NiO film on the Ni foil was 1.32 µm, and its impedance was measured 370 kΩ. However, at temperature above 900 °C, the impedance did not increase abruptly, due to the fact that the Zn^{2+} doping increased L* and prevented the impedance surge. Both observations can be compared with the uncoated foil. At 900 °C, the NiO film thickness was 1.95 µm. So both ALD

coatings provide some level of protection against oxygen at 900 ^{o}C. At temperatures above 900 ^{o}C, the coating would be dissolved in the NiO film and after the dissolution, the L* and hopping mechanism would determine the conductivity of the foils. This is why the impedance of Al_2O_3-coated foil is even higher than the uncoated foil in both *Figure 3* (b) and (c), but the impedance of ZnO-coated foil is several orders of magnitude lower.

Considering all the above observations, it seems the most effective approach in order to preserve the conductivity of Ni foils at the temperature above 900 ^{o}C is encouraging the hopping conductivity through suitable doping system, rather than keeping a physical barrier against oxygen diffusion. For example, doping with '1+' oxidation state ions with small ionic radius effectively increases the ratio of Ni^{3+}/Ni^{2+} [68]. Alkali metals, especially lithium, seem promising elements. We demonstrated the feasibility of using Li^{+} to reduce the impedance of Ni particles after sintering in other work by the authors [69,70].

4. Conclusions

The conductivity preservation of the coated Ni foils during heating to high temperatures can be divided into two parts, before and after the dissolution of the ALD coating.

Before the dissolution of ALD coatings, the mechanism that keeps the resistance low is the physical barrier between the foil and atmospheric oxygen. This barrier limits the oxygen diffusion and the formation of NiO film. As shown for the foils heated to 900 ^{o}C, thinner NiO film results in lower resistance. In this regime, the governing factors are mainly the robustness of ALD coatings (for example, one can compare the micrographs of the SnO_2 coating with the Al_2O_3 coating at 900 ^{o}C), coating thickness, and heating rate. A suitable barrier layer needs both diffusion barrier and mechanical stability (i.e. no cracking) at high temperature. The diffusion barrier will be increased by thickness, while the mechanical stability will be decreased by thickness[36]. Thus, there is an optimum thickness at which the barrier power is maximum, as shown in *Figure 2* (b) for the low heating rate. The increase of heating rate can

change the balance between diffusion barrier and mechanical stability, since the mechanical stability becomes more important than the diffusion barrier. So the optimum thickness shifts to thinner coatings, as demonstrated for the SnO_2 coatings in *Figure 3* (d).

After the dissolution of coatings, the cation diffusivity and its oxidation state are critical parameters in the Ni foil conductivity. Changing doping cations from Al^{3+} to Zn^{2+} can decrease resistance from 931 MΩ to 4 MΩ, according to the plot of *Figure 3* (c). Thus, at temperatures above 900 ^{o}C, which is necessary for sintering Ni particles, the most effective approach to preserving conductivity of Ni electrodes is choosing a suitable doping system. These findings enable the electroceramic industries to sinter their devices in higher partial pressure of oxygen without losing the conductivity of their electrode. As a result, the device would have less oxygen vacancies and consequently lower energy loss.

Acknowledgements

This material is based upon work supported by the National Science Foundation, as part of the Center for Dielectrics and Piezoelectrics under Grant Nos. IIP- 1361503 and 1361571. The authors would like to acknowledge Ms. Joanne Aller at Materials Research Institute of the Pennsylvania State University for her support in the writing process of this paper.

References

[1] Mitchell D, Sewell P and Cohen M 1976 A kinetic study of the initial oxidation of the Ni (001) surface by RHEED and x-ray emission *Surf. Sci.* **61** 355–76

[2] Giggins C and Pettit F 1971 Oxidation of Ni-Cr-Al Alloys Between 1000° and 1200° C *J. Electrochem. Soc.* **118** 1782–90

[3] Gray J E and Luan B 2002 Protective coatings on magnesium and its alloys — a critical review *J. Alloys Compd.* **336** 88–113

[4] Vilar R 1999 Laser cladding *J. Laser Appl.* **11** 64

[5] Sohrabi Baba Heidary D, Madadi F and Shamanian M 2014 Study of the Microstructures and Abrasive Characteristics of Mo-Fe-C Hardfacing Alloys Fabricated by Gas Tungsten Arc Welding *Tribol. Trans.* **58** 225–30

[6] Stratmann M, Feser R and Leng A 1994 Corrosion protection by organic films *Electrochim. Acta* **39** 1207–14

[7] Prasai D, Tuberquia J C, Harl R R, Jennings G K, Rogers B R and Bolotin K I 2012 Graphene: corrosion-inhibiting coating. *ACS Nano* **6** 1102–8

[8] Edwards R S and Coleman K S 2013 Graphene film growth on polycrystalline metals. *Acc. Chem. Res.* **46** 23–30

[9] Lahiri J, S Miller T, J Ross A, Adamska L, Oleynik I I and Batzill M 2011 Graphene growth and stability at nickel surfaces *New J. Phys.* **13** 025001

[10] Chen S, Brown L, Levendorf M and Cai W 2011 Oxidation resistance of graphene-coated Cu and Cu/Ni alloy *ACSnano* **5** 1321–7

[11] Liu Z, Gong Y, Zhou W, Ma L, Yu J, Idrobo J C, Jung J, MacDonald A H, Vajtai R, Lou J and Ajayan P M 2013 Ultrathin high-temperature oxidation-resistant coatings of hexagonal boron nitride. *Nat. Commun.* **4** 2541

[12] Dahal A and Batzill M 2014 Graphene-nickel interfaces: a review. *Nanoscale* **6** 2548–62

[13] Li L, Cervenka J, Watanabe K, Taniguchi T and Chen Y 2014 Strong oxidation resistance of atomically thin boron nitride nanosheets *ACS Nano* 1457–62

[14] Meyer J, Görrn P, Bertram F, Hamwi S, Winkler T, Johannes H-H, Weimann T, Hinze P, Riedl T and Kowalsky W 2009 Al_2O_3/ZrO_2 Nanolaminates as Ultrahigh Gas-Diffusion Barriers-A Strategy for Reliable Encapsulation of Organic Electronics *Adv. Mater.* **21** 1845–9

[15] Chou C-T, Yu P-W, Tseng M-H, Hsu C-C, Shyue J-J, Wang C-C and Tsai F-Y 2013 Transparent conductive gas-permeation barriers on plastics by atomic layer deposition *Adv. Mater.* **25** 1750–4

[16] Kim L, Kim K, Park S and Jeong Y 2014 Al_2O_3/TiO_2 Nano-Laminate Thin Film Encapsulation for Organic Thin Film Transistors via Plasma-Enhanced Atomic Layer Deposition *Appl. Mater. Interfaces* **6** 6731−6738

[17] Kim H, Cabral C, Lavoie C and Rossnagel S M 2002 Diffusion barrier properties of transition metal thin films grown by plasma-enhanced atomic-layer deposition *J. Vac. Sci. Technol. B Microelectron. Nanom. Struct.* **20** 1321

[18] Carcia P F, McLean R S, Reilly M H, Groner M D and George S M 2006 Ca test of Al_2O_3 gas diffusion barriers grown by atomic layer deposition on polymers *Appl. Phys. Lett.* **89** 031915

[19] Groner M D, George S M, McLean R S and Carcia P F 2006 Gas diffusion barriers on polymers using Al_2O_3 atomic layer deposition *Appl. Phys. Lett.* **88** 051907

[20] George S M 2010 Atomic layer deposition: an overview. *Chem. Rev.* **110** 111–31

[21] Puurunen R L 2005 Surface chemistry of atomic layer deposition: A case study for the trimethylaluminum/water process *J. Appl. Phys.* **97** 121301

[22] Haugsrud R 2003 On the high-temperature oxidation of nickel *Corros. Sci.* **45** 211–35

[23] Sato a., Chiu Y-L and Reed R C 2011 Oxidation of nickel-based single-crystal superalloys for industrial gas turbine applications *Acta Mater.* **59** 225–40

[24] Yeo H G and Trolier-McKinstry S 2014 {001} Oriented piezoelectric films prepared by chemical solution deposition on Ni foils *J. Appl. Phys.* **116** 014105

[25] Randall C A, Kelnberger A, Yang G Y, Eitel R E and Shrout T R 2005 High Strain Piezoelectric Multilayer Actuators - A Material Science and Engineering Challenge *J. Electroceramics* **14** 177–91

[26] Kobayashi K, Doshida Y, Mizuno Y and Randall C A 2012 A Route Forwards to Narrow the Performance Gap between PZT and Lead-Free Piezoelectric Ceramic with Low Oxygen Partial Pressure Processed $(Na_{0.5}K_{0.5})NbO_3$ ed D Damjanovic *J. Am. Ceram. Soc.* **95** 2928–33

[27] Kawada S, Kimura M, Higuchi Y and Takagi H 2009 $(K,Na)NbO_3$ -Based Multilayer Piezoelectric Ceramics with Nickel Inner Electrodes *Appl. Phys. Express* **2** 111401

[28] Müller A, Herbstritt D and Ivers-Tiffée E 2002 Development of a multilayer anode for solid oxide fuel cells *Solid State Ionics* **152-153** 537–42

[29] Wang Z, Qian J, Cao J, Wang S and Wen T 2007 A study of multilayer tape casting method for anode-supported planar type solid oxide fuel cells (SOFCs) *J. Alloys Compd.* **437** 264–8

[30] Kishi H, Mizuno Y and Chazono H 2003 Base-Metal Electrode-Multilayer Ceramic Capacitors: Past, Present and Future Perspectives *Jpn. J. Appl. Phys.* **42** 1–15

[31] Im D-H, Hyun S-H, Park S-Y, Lee B-Y and Kim Y-H 2006 Preparation of Ni paste using binary powder mixture for thick film electrodes *Mater. Chem. Phys.* **96** 228–33

[32] Yamamatsu J, Kawano N, Arashi T, Sato A, Nakano Y and Nomura T 1996 Reliability of multilayer ceramic capacitors with nickel electrodes *J. Power Sources* **60** 199–203

[33] Lee J-Y, Lee J-H, Hong S-H, Lee Y K and Choi J-Y 2003 Coating $BaTiO_3$ Nanolayers on Spherical Ni Powders for Multilayer Ceramic Capacitors *Adv. Mater.* **15** 1655–8

[34] Kim H G, Park J-I and Lee G H 2013 Fabrication of Ni electrode films by sintering Ni nanoparticle pastes: Compositional dependence of specific resistance and optimal composition *Mater. Chem. Phys.* **140** 419–26

[35] Lin C C, Wei W C J, Su C Y and Hsueh C H 2009 Oxidation of Ni electrode in $BaTiO_3$ based multilayer ceramic capacitor (MLCC) *J. Alloys Compd.* **485** 653–9

[36] Sohrabi Baba Heidary D, Qu W and Randall C A 2015 Evaluating the Merit of ALD Coating as Barrier against Hydrogen Degradation in Capacitors Components *RSC Adv.* **5** 50869

[37] Sohrabi Baba Heidary D and Randall C A 2015 Analysis of the degradation of $BaTiO_3$ resistivity due to hydrogen ion incorporation: Impedance spectroscopy and diffusion analysis *Acta Mater.* **96** 344–51

[38] Sohrabi Baba Heidary D, Qu W and Randall C A 2015 Electrical characterization and analysis of the degradation of electrode Schottky barriers in $BaTiO_3$ dielectric materials due to hydrogen exposure *J. Appl. Phys.* **117** 124104

[39] Sohrabi Baba Heidary D and Randall C A 2015 Evaluation of Atomic Layer Deposition coating as gas barrier against hydrogen gas and humidity *Scr. Mater.* **107** 30–3

[40] Jen S H, George S M, McLean R S and Carcia P F 2013 Alucone interlayers to minimize stress caused by thermal expansion mismatch between Al_2O_3 films and Teflon substrates *ACS Appl. Mater. Interfaces* **5** 1165–73

[41] Jen S-H, Bertrand J a. and George S M 2011 Critical tensile and compressive strains for cracking of Al_2O_3 films grown by atomic layer deposition *J. Appl. Phys.* **109** 084305

[42] Sadeghi-Tohidi F, Samet D, Graham S and Pierron O N 2014 Comparison of the cohesive and delamination fatigue properties of atomic-layer-deposited alumina and titania ultrathin protective coatings deposited at 200 °C *Sci. Technol. Adv. Mater.* **15** 015003

[43] Yesibolati N, Shahid M, Chen W, Hedhili M N, Reuter M C, Ross F M and Alshareef H N 2014 SnO_2 anode surface passivation by atomic layer deposited HfO_2 improves li-ion battery performance *Small* **10** 2849–58

[44] Choi D and Park J-S 2014 Highly conductive SnO_2 thin films deposited by atomic layer deposition using tetrakis-dimethyl-amine-tin precursor and ozone reactant *Surf. Coatings Technol.* **259** 238–43

[45] Varela J A, Perazolli L A, Longo E, Leite E R and Cerri J A 2002 Effect of atmosphere and dopants on sintering of SnO_2 *Sci. Sinter.* **34** 23–31

[46] Polotai A, Breece K, Dickey E, Randall C and Ragulya A 2005 A Novel Approach to Sintering Nanocrystalline Barium Titanate Ceramics *J. Am. Ceram. Soc.* **88** 3008–12

[47] Yan Z, Martin C L, Guillon O, Bouvard D and Lee C S 2014 Microstructure evolution during the co-sintering of Ni/$BaTiO_3$ multilayer ceramic capacitors modeled by discrete element simulations *J. Eur. Ceram. Soc.* **34** 3167–79

[48] Ragulya a. V. and Skorokhod V V. 1995 Rate-controlled sintering of ultrafine nickel powder *Nanostructured Mater.* **5** 835–43

[49] Yoon J R, Shin D S, Jeong D Y and Lee H Y 2012 Control of connectivity of Ni electrode with heating rates during sintering and electrical properties in $BaTiO_3$ based multilayer ceramic capacitors *Trans. Electr. Electron. Mater.* **13** 181–4

[50] Jo G, Lee K and Kang S L 2013 Effect of Passivation on the Sintering Behavior of Submicron Nickel Powder Compacts for MLCC Application *J. Korean Powder Metall. Inst.* **20** 405–10

[51] Nowotny J and Sadowski a. 1979 Chemical Diffusion in Nickel Oxide *J. Am. Ceram. Soc.* **62** 24–8

[52] Austin I G and Mott N F 2001 Polarons in crystalline and non-crystalline materials *Adv. Phys.* **50** 757–812

[53] Honig J 1966 Electrical properties of metal oxides which have“ hopping” charge carriers *J. Chem. Educ.* **43** 76–82

[54] Snowden D and Saltsburg H 1965 Hopping conduction in NiO *Phys. Rev. Lett.* **1** 13–5

[55] Williams D B and Carter. C B 2009 *Transmission Electron Microscopy: A Textbook for Materials Science* (New York: Springer)

[56] Evans C, Brundle R and Wilson S 1992 *Encyclopedia of Materials Characterization* (Amsterdam: Elsevier)

[57] Badev A, Marinel S, Heuguet R, Savary E and Agrawal D 2013 Sintering behavior and non-linear properties of ZnO varistors processed in microwave electric and magnetic fields at 2.45GHz *Acta Mater.* **61** 7849–58

[58] Nasu N, Tsuda K, Siratori A and Fujimori K 2000 *Electronic Conduction in Oxides* (Berlin: Springer)

[59] Antoini E 1992 Sintering of $Li_xNi_{1-x}O$ solid solutions at 1200 °C *J. Mater. Sci.* **27** 3335–40

[60] Tyuliev G and Sokolova M 1991 Temperature dependence of Ni^{3+} quantity in the surface layer of NiO *Appl. Surf. Sci.* **52** 343–9

[61] Voleník K, Ctibor P, Dubský J, Chráska P and Horák J 2004 Oxidation of nickel during plasma spraying and some properties of nickel oxide *Czechoslov. J. Phys.* **54** C889–96

[62] Lunkenheimer P, Loidl A, Ottermann C and Bange K 1991 Correlated barrier hopping in NiO films *Phys. Rev. B* **44** 2–5

[63] Ahn C C 2004 *Transmission Electron Energy Loss Spectrometry in Materials Science and the EELS Atlas* (Weinheim: Wiley-VCH)

[64] Muto S, Sasano Y, Tatsumi K, Sasaki T, Horibuchi K, Takeuchi Y and Ukyo Y 2009 Capacity-Fading Mechanisms of $LiNiO_2$-Based Lithium-Ion Batteries *J. Electrochem. Soc.* **156** A371

[65] Von Harrach H, Klenov D, Freitag B, Schlossmacher P, Collins P and Fraser H 2010 Comparison of the Detection Limits of EDS and EELS in S/TEM *Microsc. Microanal.* **16** 1312–3

[66] Swaroop S, Kilo M, Argirusis C, Borchardt G and Chokshi A H 2005 Lattice and grain boundary diffusion of cations in 3YTZ analyzed using SIMS *Acta Mater.* **53** 4975–85

[67] Cerri J A, Leite E R, Gouvêa D, Longo E and Varela J A 2005 Effect of Cobalt(II) Oxide and Manganese(IV) Oxide on Sintering of Tin(IV) Oxide *J. Am. Ceram. Soc.* **79** 799–804

[68] Guo W, Hui K N and Hui K S 2013 High conductivity nickel oxide thin films by a facile sol–gel method *Mater. Lett.* **92** 291–5

[69] Sohrabi Baba Heidary D and Randall C Preserving nickel electrode conductivity during sintering process using lithium carbonate coatings *Submitted*

[70] Sohrabi Baba Heidary D and Randall C A Coating Ni particles to preserve their conductivity during sintering at oxidizing atmospheres *Submitted*